AAEC/E602

AAEC/E602

AUSTRALIAN ATOMIC ENERGY COMMISSION

RESEARCH ESTABLISHMENT

LUCAS HEIGHTS RESEARCH LABORATORIES

THE AAEC ROTAMAK EXPERIMENT DESCRIPTION AND PRELIMINARY RESULTS AT LOW INPUT POWER

by

G. DURANCE

G.R. HOGG

J. TENDYS

DECEMBER 1984

ISBN 0 642 59817 7

AUSTRALIAN ATOMIC ENERGY COMMISSION
RESEARCH ESTABLISHMENT

LUCAS HEIGHTS RESEARCH LABORATORIES

THE AAEC ROTAMAK EXPERIMENT DESCRIPTION AND PRELIMINARY RESULTS AT LOW INPUT POWER

by

G. DURANCE
G.R. HOGG
J. TENDYS

ABSTRACT

A description is given of the initial experiments on a rotamak device operating with 10 kW input power at a frequency of 1.85 MHz. The experimental apparatus and the diagnostic systems are also described. The matching of the radiofrequency power sources to the drive coils is discussed and details are given of the results from discharges in hydrogen, deuterium, helium and argon. The plasma/magnetic field configuration appears to be stable although, under certain conditions, fluctuations of the magnetic field structure have been observed.

National Library of Australia card number and ISBN 0 642 59817 7

The following descriptors have been selected from the INIS Thesaurus to describe the subject content of this report for information retrieval purposes. For further details please refer to IAEA-INIS-12 (INIS: Manual for Indexing) and IAEA-INIS-13 (INIS: Thesaurus) published in Vienna by the International Atomic Energy Agency.

PLASMA; TOKAMAK DEVICES; COMPACT TORUS; MAGNETIC FIELDS; ELECTRIC CURRENTS; RF SYSTEMS; ELECTRIC DISCHARGES; HYDROGEN; DEUTERIUM; HELIUM; ARGON; EXPERIMENTAL DATA

CONTENTS

1. INTRODUCTION

In the rotamak concept [Jones 1979], a rotating magnetic field is used to generate and maintain the steady toroidal current and its associated poloidal magnetic field in a steady-state compact toroid configuration. Experimentally, the rotating field is obtained by feeding RF currents of the same amplitude and frequency, but dephased by 90°, into two orthogonal Helmholtz coils located around the outside of a spherical non-conducting discharge vessel. An additional externally-generated magnetic field perpendicular to the toroidal plane must be provided for plasma equilibrium. By analogy with tokamaks, this latter field will be referred to as the 'vertical' field. The resultant poloidal magnetic field consists of a combination of closed and open poloidal field lines as shown in figure 1. In nearly all of the rotamak research undertaken so far no toroidal magnetic field has been provided.

The initial rotamak experiments were carried out at Flinders University where a series of high-power, short duration (~ few MW of radiofrequency (RF) power for some tens of microseconds) experiments and some complementary low-power, long duration (~ few kW of RF power for ~ ten milliseconds) experiments were undertaken [Hugrass *et al.* 1980; Durance *et al.* 1982a,b; Durance 1982; Jessup and Tendys 1982; Tendys and Turley 1983]. These experiments proved that the desired compact torus configuration could indeed be achieved and maintained for the duration of the rotating magnetic field. Furthermore, the configurations appeared remarkably stable. Although these results are encouraging, many issues have yet to be addressed before the potential of the rotamak concept can be realistically assessed. For example, energy and particle confinement times are presently unknown; ion spin-up has yet to be investigated; and, in the longer term, methods of supplementary heating will have to be examined. In an endeavour to obtain information on these and other issues, rotamak experiments are being undertaken jointly at the Flinders University of South Australia and at the Lucas Heights Research Laboratories.

In both laboratories, two RF current sources each with an output of ~ 100 kW will be used to produce the rotating magnetic field for future experiments.

At Lucas Heights, the low-power stages (with a combined RF output power of ~ 10 kW) have been assembled and tested. This report describes the low-power stages and associated experiments. The limited diagnostic equipment presently available has placed constraints on the physics parameters which have been investigated.

2. EXPERIMENTAL APPARATUS

2.1 Discharge Vessel and Vacuum System

The spherical Pyrex glass discharge vessel is 0.28 m in diameter, and has two diametrically opposed pumping ports (0.085 m diameter). A schematic diagram of the experimental apparatus is shown in figure 2a. An axial glass tube (~ 6 mm o.d.) provides access for probes and radial access is provided in the equatorial toroidal plane by two ports, each equipped with a retractable glass probe-guide (5.6 mm o.d., 3.6 mm i.d.). Further access is provided by an array of 23 retractable probe-guides (4 mm o.d., 2.2 mm i.d.) spaced 1 cm apart although these guides have not been used in the present experiments. Special access is also provided for a Rogowski coil to measure the toroidal current (figure 2b). A 4 in. oil diffusion pump with liquid nitrogen trap is used to evacuate the vessel. A gate valve is also provided to isolate the discharge vessel from the pumping system.

The continuous flow of filling-gas was originally controlled by a piezo-electric valve (Veeco model PV10). However, the voltage supply for this valve was susceptible to RF interference which resulted in the valve occasionally closing during the preionisation pulse. To maintain a steady filling pressure, continual adjustment of the valve voltage supply was required. To overcome such problems, this valve has recently been replaced by a manually controlled needle valve.

The base pressure (0.1 mPa) and the filling pressure (typically ~ 120 mPa for hydrogen) are monitored by an ionisation gauge (Varian Model 564) and controller (Varian model 890-AR). The pressures quoted in this report have been corrected for the relative gauge sensitivity for the different gases.

2.2 RF Current Generation

The RF power sources are indicated schematically in figure 3. Since the linear amplifiers were originally intended for use in the amateur radio bands, their lower frequency limit is ~ 1.8 MHz. For the present experiments the system was operated at a frequency of 1.85 MHz. The duration of the RF current pulse was

limited to ~ 15 ms to avoid the necessity of cooling the Helmholtz coils and RF matching networks. The impedance matching circuit used to couple the final amplifier to the Helmholtz coils is shown in figure 4.

2.3 Helmholtz Coils

The rotating magnetic field is generated by feeding two RF current pulses (dephased by 90°) into a pair of orthogonal Helmholtz coils. Each Helmholtz coil is made from 2.5 mm o.d. enamelled copper wire insulated with nylon tube and formed into two coil sections each of three turns (approximate coil diameter 0.3 m). The coils are supported by Perspex collars mounted on the outside of the spherical Pyrex glass discharge vessel. The vacuum inductance of each Helmholtz coil is ~ 15 μH.

Although the two Helmholtz coils are nominally orthogonal, there is nevertheless a small mutual inductance of several hundred nanohenries between them. This has to be eliminated in order that the two impedance-matching circuits can be adjusted independently. This has been achieved by coupling the two circuits with a small variable mutual inductor formed by two loops with an adjustable separation. By appropriately adjusting this mutual inductance it is possible to make the net coupling between the two RF drive circuits sufficiently small.

The presence of plasma changes the impedance of the Helmholtz coils. In practice the variable capacitor in each impedance matching circuit is adjusted with a plasma present in the vessel for maximum power transfer to the Helmholtz coils.

2.4 Equilibrium Vertical Field

An externally imposed magnetic field, the vertical field, is required to maintain plasma equilibrium and is produced by two coils of mean diameter 0.3 m positioned symmetrically about the discharge vessel with a separation of 0.5 m. Each coil has 10 turns (actually double wound with 2.5 mm diameter enamelled copper wire) wound on a circular Perspex former.

Current is supplied to the coils by the circuit described by Watt [1983]. The rise-time, amplitude and duration of the current waveform are all adjustable.

2.5 Preionisation

At the range of filling pressures used, the main RF discharge is insufficient to ionise the filling gas. This problem is overcome by weakly preionising the gas by passing a RF current pulse through two coils of six turns each wound on the two pumping arms. The output of an Airmec type 304A oscillator switched by a reed relay into a 300 W ENI A-300 broadband power amplifier is used to supply the RF current. The duration of the pulse is limited to ~ 1 second before the main RF discharge. Some overlap (typically ~ 1 ms of the preionisation and the main discharge) is necessary.

The preionisation configuration is somewhat arbitrary, and has been based on a similar system at Flinders University. It is successful in preionising hydrogen down to filling pressures of the order of ~ 100 mPa.

The optimum oscillator frequency depends on the type of filling gas and on the filling pressure. Frequencies in the range ~ 17-23 MHz have been used. It should be noted, however, that this combination of frequency and pulse duration has proved to be a continuing source of interference to most of the electrical and electronic equipment in the laboratory. Although screening and, in particular, cable layout have eliminated many of the problems, an alternative means of preionisation would still be desirable.

2.6 Timing and Trigger Circuits

A series of pre-set but variable timing circuits have been assembled to permit triggering of the preionisation RF drive, the main RF drive system, vertical field power supply and diagnostic oscilloscopes at the required times.

2.7 Screened Rooms

Two double screened rooms have been constructed, each with its own filtered mains supply. One room (1.5 m x 2.2 m x 2.2 m high) contains the low power RF drive unit, the vertical field supply and timing units together with oscilloscopes for measuring the RF drive signals. The larger room (4.0 m x 2.2 m x 2.2 m high) is used exclusively for diagnostic data processing and collection. The two rooms are only connected at the mains supply earth point.

3. DIAGNOSTICS

3.1 Introduction

At this stage, the diagnostics have been limited to measurements of the total driven toroidal current and various magnetic field components. Since the currents and fields in the present experiment are small, and since the configuration changes on a relatively slow time-scale (~ milliseconds), the resulting voltage signals (proportional to dI/dt and dB/dt) induced in the Rogowski coil and magnetic probes are small. This necessitates the use of many turns in the Rogowski coil and the wire-wound probes, together with signal amplification and active integration. On the other hand, the rapidly changing 1.85 MHz RF component leads to very large values of dB/dt, hence the output signals associated with this component are large.

In practice, the diagnostic circuitry has proved to be very susceptible to high-frequency pick-up of both the ~ 20 MHz preionisation pulse and the 1.85 MHz RF pulse. This has been observed to introduce d.c. offsets in the output from the signal amplifiers. Such offsets transform into ramps upon integration. Thus considerable effort has been directed to filtering out any RF components before amplification. All calibration figures quoted in the following text refer to the complete system of probe, or Rogowski coil, together with its associated amplifiers, integrators and filters.

3.2 Rogowski Coil

The Rogowski coil is threaded through a central axial glass tube and around the outer surface of the discharge vessel to enclose a complete cross-section across the minor radius of the plasma torus. The coil consists of 4720 turns of 40 S.W.G. enamelled copper wire wound on a 3.3 mm diameter plastic former with internal return wire. The coil has a resistance of 73 Ω and an inductance of 440 μH. The output signal is transferred *via* a 50 Ω triaxial cable to the Faraday cage where it is filtered, amplified and integrated. The calibration factor has been determined to be 0.84 A mV^{-1}.

3.3 Magnetic Probes

The size of the re-entrant probe ports has placed some constraint on the sizes of the probes. Conventional wire-wound probes were originally constructed and used for the early measurements. However, these have been abandoned in favour of Hall effect probes which have the advantage of not requiring integration. Two Hall probes have been constructed using Siemens SBV 566 Hall generators — one probe is suitable for measuring B_z in the radial direction, and the other measures B_z along the axis.

The sensitive area of the Hall generators is 0.9 mm × 0.9 mm and the overall size is ~ 2.5 mm × 2.5 mm excluding terminal leads. These devices are mounted on the end of 3.2 mm o.d. stainless steel tubes which provide screening for the signal leads. The radial B_z probe is electrostatically shielded with a thin (0.05 mm) copper sheath. The Hall probes are operated with an excitation current of ~ 30 mA, supplied by NiCd batteries. Temperature compensation has not been provided but probe stability appears to be adequate. The Hall probe outputs are transferred *via* triaxial cables to the Faraday cage where they are filtered and amplified, resulting in an overall probe sensitivity of ~ 0.2 G mV^{-1}.

A small probe was used to measure the rotating magnetic field B_θ. The probe coil was constructed with 40 turns of 48 S.W.G. insulated copper wire wound on a Mylar former. The coil, with dimensions 2.5 × 0.7 × 0.7 mm, was inserted into a 0.9 mm diameter stainless steel tube; a slit of approximately 3.0 × 0.25 mm was cut into the end of the tube to ensure magnetic field penetration into the coil area. The probe output was connected by triaxial cable to the Faraday cage where it was filtered (4 MHz low-pass filter) and terminated. The probe sensitivity was ~ 33 Ts^{-1} mV^{-1} at the oscilloscope.

3.4 Power Measurements

Two capacitance voltage dividers and self-integrating current transformers were constructed to measure the voltages and currents associated with each of the load circuits. They are permanently located at the input to the impedance matching circuits. A sharp cut-off elliptic low-pass filter (6 dB at 2.6 MHz) is used with each voltage probe to reduce the harmonic distortion of the signal.

The output power of the RF amplifiers has been estimated from measurements of the voltage and current probe signals displayed on an oscilloscope. The average power is

$$\overline{P} = \frac{1}{2} I_o V_o \cos\phi$$

where V_o and I_o are the amplitudes of the voltage and current signals, and ϕ is the relative phase angle between them (the phase angle is first corrected for any inherent phase shift arising from the circuitry). Typically, the measured input power into *each* of the two impedance matching transformers is ~ 4-6 kW. At present the fraction of this power dissipated within the load circuitry has not been determined with sufficient precision.

3.5 RF Current Monitors

An Ion Physics Corporation model CM-2.5-S current transformer is used to monitor the current in each Helmholtz coil. The output signals from these transformers provide information on the rotating magnetic field. A circuit to monitor the phase difference between the two currents for the duration of the discharge is under construction.

3.6 Spectroscopy

A Jarrell-Ash 0.25 m Ebert monochromator has been used for preliminary spectroscopic investigations. To avoid RF interference problems, the monochromator has been located with its photomultiplier and power supply in a screened room, and a fibre optic light pipe used to transport the plasma light onto the entrance slit of the monochromator. The spectral response of the complete system has not been determined absolutely.

4. EXPERIMENTAL MEASUREMENTS

The following procedure is used to optimise the RF current generation:

(i) Each amplifier chain is tuned in turn to give a maximum power output into a 50 Ω resistive load.

(ii) The mutual coupling between the Helmholtz coils is minimised by adjusting the coupling between the mutual inductance loops.

(iii) The phasing of the input signal into each amplifier chain is adjusted to give a relative phase difference of 90°.

(iv) The impedance matching stages are tuned by monitoring the voltage and current signals into each matching circuit and adjusting the variable capacitor until the circuits appear resistive (*i.e.* voltage and current signals are in phase and power transfer is at a maximum). This is performed with the discharge vessel evacuated, and the power turned down to avoid voltage breakdowns since the unloaded Q of the output unit is quite high.

(v) Fine tuning is accomplished by repeating the previous two steps at full power, but this time with plasma discharges.

During experiments, the amplitudes of the RF currents in the Helmholtz coils are routinely monitored. The amplitudes are approximately constant throughout each discharge (see figure 5). Spot checks on the relative phasing of the two RF currents are also performed.

The majority of experiments were performed using hydrogen as the experimental gas, but some experiments were carried out with deuterium, helium and argon. With the present preionisation scheme, there is a lower limit to the filling pressure at which each of the gases produces reliable discharges, ranging from 30 mPa for argon to 500 mPa for helium.

4.1 Hydrogen Discharges

The driven toroidal current was first recorded for a range of filling-gas pressures and applied vertical field amplitudes. The driven toroidal current, I_θ, was observed to increase with the applied vertical field. However, the very close correlation observed at Flinders University where, in argon discharges, the I_θ and the vertical field waveforms were essentially identical in shape, has not been observed in these present experiments (for example, see figure 8). Since the correlation improved at lower filling pressures, the high atom densities in these present hydrogen experiments might have played a significant role. This is supported by the observation that, for a given applied vertical field, the driven current decreased with increasing filling pressure as shown in figure 6. In this case, a linearly ramped vertical magnetic field was applied. It is also observed that the H_β emission increased with filling pressure.

At low filling pressures (130 mPa), the driven current was cut off sharply as the vertical field decayed, even though the rotating magnetic field was still being applied (see figure 6a). At higher filling pressures

this sharp cut-off was not observed (see figure 6b).

Some preliminary gas-puffing experiments were performed with an additional 'puff' of gas introduced during the discharge. The effects of different quantities of gas and different times of introduction were investigated. With gas-puffing, the driven current decreased slightly (similar to the decrease observed at higher initial filling pressures), and the early termination of the current discussed in the preceding paragraph, was avoided. No other effects were discernible. In these experiments, the same piezo-electric valve was used for both the continuous gas bleed and the superimposed puff. It was necessary to readjust the valve supply voltage after every discharge to maintain the same steady gas flow. It should be noted that the valve was located in the main pumping arm, some distance from the spherical discharge vessel, thus the gas was not puffed directly into the plasma.

For any given initial gas filling pressure, there was a limit to the maximum amount of current which could be driven. (Some limit can be expected on the basis of the limited available RF input power.) Endeavours to exceed this maximum by further increasing the vertical field resulted in the driven current cutting off completely even though the rotating field was still being applied. A maximum driven current of $\sim$ 250 A was observed. Under some conditions, partial rather than complete current cut-off was observed (see figure 7). In such cases, the driven current recovered towards the end of the discharge.

More detailed investigations were carried out for several applied vertical fields with different rise times and amplitudes, choosing the lowest filling pressure capable of producing reliable discharges. One representative set of results is given in figures 8-12. The radial and axial magnetic probe measurements of the z-component of the magnetic field ($B_z(r,0)$ and $B_z(0,z)$) are shown in figures 9-10 at a selected time during the discharge. Also shown are the corresponding poloidal fluxes:

$$\psi(r, 0) = 2\pi \int_0^r r' B_z(r', 0)\, dr'$$

The radial position of the separatrix and the axial positions of the neutral points are shown in figure 8.

The radial distribution of the θ-component of the rotating magnetic field, $B_\theta(r,0)$, was measured with the miniature wire-wound probe. A representative result is shown in figure 11 at a selected time during the discharge. The equivalent distribution of $B_\theta(r,0)$ in the absence of a plasma but with the same coil currents is also indicated in figure 11. The slight variation in Helmholtz coil currents throughout a discharge (see figure 5b) has not been taken into account.

The intensities of the hydrogen spectral lines at 486.1, 434.0, 410.2 and 397.0 nm were recorded as functions of time during the discharge (see, for example, figure 12). No other spectral lines were discernible. However the spectral response of the system was limited at short wavelengths by the Pyrex vessel and light pipe and at long wavelengths by the photomultiplier. Helium was added to the hydrogen filling gas, and estimates of the electron temperature obtained using the helium singlet-to-triplet ratio method [Huddlestone & Leonard 1965]. The percentage of helium was gradually increased in successive discharges up to $\sim$ 30 per cent, maintaining a constant total filling pressure. The recorded intensities of the 471.3 and the 492.1 nm spectral lines showed the expected linear dependence with helium filling pressure. The singlet-to-triplet ratio was essentially constant (varying from $\sim$ 1.3 to $\sim$ 1.5) over this range. This implies an electron temperature $\sim$ 12 eV. However, this method is known to be subject to a number of serious limitations. At best, the predicted temperature can be regarded as a very approximate estimate. No HeII spectral lines were observed in these discharges.

Under certain conditions, fluctuations of the magnetic field structure were observed. These fluctuations generally appeared whenever the driven toroidal current exceeded $\sim$ 220 A although at low initial filling pressures, currents up to $\sim$ 250 A were observed without magnetic field fluctuations. The dominant frequency component of the magnetic fields was $\sim$ 50 kHz with higher harmonics also being present. These fluctuations were readily apparent on all the magnetic probe signals. They were also present on the Rogowski current signal (see figure 7) but with a relatively small amplitude that is probably attributable to filtering in the integrator circuitry. The fluctuations did not appear to be totally disruptive, but if the 'mean' driven current exceeded $\sim$ 230 A, the current was observed to cut off either completely or partially. During a partial cut-off phase (figure 7), the fluctuations were very apparent with a dominant frequency of $\sim$ 10 kHz, though higher harmonics were again present. In the case shown in figure 7, the driven current is seen to recover. For the same filling pressure and vertical field amplitude, the onset of the magnetic field fluctuations, their frequency, the onset of I_θ cut-off, the fluctuation frequency during cut-off, and the

recovery were all highly reproducible. Gas puffing during a discharge prevented the I_θ cut-off phase, but did not affect the ~ 50 kHz oscillations.

4.2 Deuterium, Helium and Argon Discharges

Deuterium and helium discharges were very similar to the hydrogen discharges (see figures 13-14). The onset of magnetic field fluctuations appeared to be the same (*i.e.* when I_θ exceeds ~ 220 A). The fluctuations in these cases appeared more noise-like with no obvious dominant frequencies. Electron temperature estimates, based on the helium singlet-to-triplet ratio method, were in the range 10-15 eV.

In argon, it was possible to obtain rotamak discharges at considerably lower gas-filling pressures than for other gases. A maximum driven current of ~ 600 A was achieved and the plasma size was significantly larger. A typical set of argon results are shown in figures 15-19.

The magnetic field fluctuations with argon were also different. Under appropriate conditions, the probe signals were oscillatory and relatively free of harmonic contamination and 'noise'. Three distinct regimes of fluctuations were produced by applying a ramping vertical field and varying the filling pressure (see figure 20):

(i) A ~ 20-40 kHz oscillation was observed during the initial current rise (onset when I_θ exceeds ~ 170 A). This oscillation lasted for ~ 1 ms. It occurred only at low filling pressures (< 25 mPa) and appeared to be associated with the plasma separatrix coming off the vessel wall.

(ii) A ~ 200 kHz oscillation occurred later in the current rise (onset when I_θ ~ 300 A) and persisted until the driven current started to decay at the end of the ramping vertical field. This oscillation occurred only for filling pressures within the range ~ 60-90 mPa. It appeared to be related to the oscillations observed with the other gases.

(iii) A ~ 16 kHz oscillation was observed during the decay of the driven current as the vertical field decayed (onset occurred when I_θ fell to ~ 200 A). This oscillation appeared at filling pressures similar to those required for the ~ 200 kHz oscillation and seemed to be associated with the different decay rates of the driven current and the vertical field.

5. ESTIMATES OF PLASMA PARAMETERS

The electron number density was not been measured in these experiments. However it is possible to obtain a lower bound by assuming that all the electrons rotate synchronously with the rotating field. This enables the total number of electrons, N, to be deduced from the measured toroidal current, I_θ, and the rotating field frequency, f, *i.e.* from

$$I_\theta = Nef$$

where e is the electron charge. Assuming that all these N electrons are contained within the separatrix, the average electron number density can be estimated. In these present experiments, the resulting density estimates range from ~ 2.2×10^{17} to ~ 4.4×10^{17} m^{-3}. Since the original atom filling density ranges from ~ $(0.7\text{-}1.0) \times 10^{19}$ m^{-3} for argon to ~ $(5\text{-}10) \times 10^{19}$ m^{-3} for hydrogen, the percentage of the original atom filling density that is actually ionised is seen to be very small (from ~ 2.5-5 per cent for argon down to < 1 per cent for hydrogen and the other gases). Such a weakly ionised plasma is expected to have a very low temperature (< 1 eV). However, it is possible for the neutral atoms within the plasma to be heated, leading to a decrease in density (from pressure balance), and substantial decreases in neutral atom number densities have been claimed in some plasmas.

Taking 3×10^{17} m^{-3} as a representative electron number density and pessimistically taking 10^{20} m^{-3} as the neutral atom number density, enables various plasma parameters to be estimated (see table 1). It is assumed in table 1 that that $n_i \sim n_e$. Since the electron temperature has not been accurately determined, the parameters in table 1 have been calculated for $T_e = 1$ eV and $T_e = 10$ eV even though the latter value would appear to be incompatible with high neutral concentrations. Therefore it must be emphasised that the values of the parameters shown in table 1 are intended as a guide only.

The estimated Debye length and the number of particles in the Debye sphere clearly indicate that a 'plasma' was present in these experiments.

For a rotating magnetic field of ~ 7 G, the following estimates for the ion and electron cyclotron frequencies can be made:

$$\omega_{ci} \sim 6.7 \times 10^4 \text{ rad s}^{-1} \text{ (for hydrogen ions)}$$

$$\omega_{ce} \sim 1.2 \times 10^8 \text{ rad s}^{-1}$$

(ω_{ci} would be smaller for the other types of ions). The angular frequency of the rotating magnetic field, ω, in these experiments is $\sim 1.2 \times 10^7$ rad s^{-1}. Thus the conditions for current drive by the rotating field technique are seen to be fulfilled, namely:

$$\omega_{ci} << \omega << \omega_{ce}$$

$$\nu_{ei}, \nu_{en} << \omega_{ce}$$

6. APPLICABILITY OF THE SOLOV'EV MODEL

We now examine the applicability of the Solov'ev model to describe the plasma equilibria. Axisymmetric toroidal equilibria are described generally by the Grad-Shafranov equation. Solov'ev [1976] has given a simple *analytic* solution of this equation for a particular class of equilibria. A form of the Solov'ev solution reads

$$\psi(r,z) = \frac{r^2 B_a}{2}\left[\frac{r^2}{R^2} + \frac{\varepsilon^2 z^2}{R^2} - 1\right]$$

where $B_a = B_z(0,0)$, R is the position of the separatrix on the r-axis, and $\varepsilon = R/Z_x$ where Z_x is the position of the neutral point on the z-axis. The maximum value of $\psi(r,z)$ occurs at the magnetic axis, *i.e.* at $r = R/\sqrt{2}$, $z=0$. For the solution given above, it follows that

$$\frac{\psi(r,0)}{\psi(R/\sqrt{2},0)} = 4(r/R)^2\,[1-(r/R)^2]$$

This relationship is plotted in figure 21 together with the experimental data corresponding to the argon discharge of figure 16 (at t = 12 ms), and to the hydrogen discharge of figure 8 (at t = 12 ms). The experimental data agree well with the Solov'ev solution. Taking the following experimental data, the Solov'ev solution can now be used to predict further plasma parameters.

	Hydrogen	Argon
I_θ (A)	230	450
R (m)	0.09	0.13
Z_x (m)	0.058	0.10
ε	1.55	1.3

		Hydrogen	Argon
$B_z(0,0)$	(G)	12.2	14.9
n_e	(m^{-3})	4.1×10^{17}	2.1×10^{17}
T_e^{max}	(eV)	14	36

The maximum electron temperature has been calculated assuming that $T_i \sim 0$. In view of the long equilibration time (see table 1), this assumption may be justified for an argon plasma, but is not valid for a hydrogen plasma where some ion heating would be expected.

Comparing the predicted $B_z(0,0)$ values with the experimental values of figures 8 and 17, it is seen that reasonable agreement is achieved in the argon case (experimental $B_z(0,0) \sim$ 11-12 G), but that there is a large discrepancy in the hydrogen case (experimental $B_z \sim$ 3-5 G). This casts doubt on the applicability of the Solov'ev solution to the present hydrogen experiments despite the apparently good agreement exhibited in figure 20.

7. DISCUSSION

For the hydrogen results shown in figure 8, the driven current is observed to rise rapidly to a peak, fall slightly, and then rise more slowly. The measured positions of the magnetic axis and neutral points imply that the plasma contracts rapidly to a minimum size, and then relaxes outwards slightly — the minimum size corresponding approximately to the minimum in the driven current. It appears that initially the driven current rises more slowly than the applied vertical field, leading to compression of the plasma spheroid by the vertical field. As the compression proceeds, it is accompanied by a decrease in the driven current. This must arise from either an enhanced particle loss mechanism or an increase in the slip between the driven electron fluid and the rotating magnetic field. This continues until the applied vertical field ceases to rise, whereupon the driven current is observed to increase gradually again accompanied by an increase in the plasma size (figure 8).

A somewhat similar situation prevails when the vertical field decays. The decay rate of this field appears to be faster than that of the driven current, leading to an expansion of the plasma (figure 8).

It is evident that complete penetration of the rotating field into the plasma was not achieved in these experiments. However, only a few per cent slip between the electron fluid and the rotating magnetic field is required to explain the observed results. From figure 11, the effective skin depth, δ^*, in the plasma is ~ 4.5 cm. From table 1, the expected classical skin depth, δ, is ~ 1 cm. The effective skin depth is related to the classical skin depth as follows [Hugrass 1979]:

$$\delta^* = \delta[1 - \frac{v_{eo}}{v_{ph}}]^{-\frac{1}{2}}$$

where v_{eo} is the electron drift velocity in the θ-direction and v_{ph} is the phase velocity of the field. Therefore

$$(1 - \frac{v_{eo}}{v_{ph}}) = (\delta/\delta^*)^2 = 0.05$$

Thus only ~ 5 per cent slip between the electron fluid and the rotating magnetic field is required to explain the observed results. In figure 11, there is evidence of a layer of screening currents just inside the vessel wall, as well as a layer on the surface of the plasma spheroid.

The role that the neutral atoms play in these low power rotamak experiments has not been clearly established. It is clear, however, that they do have some effect on the discharge. This is seen in figure 15, where the driven current in an argon plasma is shown at two different initial gas filling pressures with the same applied vertical field. Only at the lower filling pressure is there a close correlation between the driven current and the applied vertical field. The initial atom filling densities for the other gases were typically an order of magnitude greater than for the argon experiments. This may, at least partially, explain the lack of close correlation between the driven current and the applied vertical field in the hydrogen experiments, and may also account for the driven current being lower in hydrogen than in argon for the same applied vertical field. Better preionisation is really required to permit operation with lower initial filling densities.

8. CONCLUSIONS

Plasmas with a compact torus configuration have been produced in the present low-power AAEC rotamak experiments with a rotating magnetic field frequency of 1.85 MHz.

The reason for the relatively small plasma size in the case of hydrogen, deuterium and helium plasmas is not completely understood, but is associated with the fact that the toroidal currents driven in these cases were smaller than the corresponding current in argon (for the same applied vertical field).

The Solov'ev equilibrium model may be applicable to the argon results, but it does not appear to be applicable to the hydrogen results.

Under certain conditions, fluctuations of the magnetic field structure have been observed in these experiments. The mechanisms driving these oscillations are not presently understood.

However, under most conditions, the plasma/field configurations appear remarkably stable. The role that the possibly high neutral atom concentration plays with regard to the equilibrium and stability characteristics of these present experiments is not known.

9. ACKNOWLEDGEMENTS

The authors wish to acknowledge the interest taken in this project by Professor I.R. Jones and the many discussions they have had with him. The support given by Dr J.K. Parry is also acknowledged.

10. REFERENCES

Durance, G. [1982] - A high-power, short-duration rotamak experiment. *American Physical Society Meeting on Plasma Physics, New Orleans. Bull. Am. Phys. Soc.,* 27:932.

Durance, G., Jessup, B.L., Jones, I.R. and Tendys, J. [1982a] - Experimental observations of rotamak equilibria. *Phys. Rev. Lett.,* 48:1252.

Durance, G., Jones, I.R., Tendys, J. and Turley, M. [1982b] - Recent results from the rotamak experiments. *Proc. Ninth Int. Conf. on Plasma Physics and Controlled Nuclear Fusion Research,* Baltimore. USA. Paper IAEA-CN-41/W-10.

Huddlestone, R.H. and Leonard, S.L. (Ed.) [1965] - Plasma Diagnostic Techniques. Academic Press, New York, p.254.

Hugrass, W.N. [1979] - Production of plasma currents using transverse rotating magnetic fields. Ph.D Thesis; The Flinders University of South Australia.

Hugrass, W.N., Jones, I.R., McKenna, K.F., Phillips, M.G.R., Storer, R.G. and Tuczek, H. [1980] - Compact torus configuration generated by a rotating magnetic field: the rotamak. *Phys. Rev. Lett.,* 44:1676.

Jessup, B.L. and Tendys, J. [1982] - Low power, long duration rotamak discharges in argon. Flinders University Report, FUPH-R-180.

Jones, I.R. [1979] - The rotamak concept. Flinders University Report, FUPH-R-151.

Solov'ev, L.S. [1976] - In *Reviews of Plasma Physics.* Consultants Bureau, New York. 6:239.

Tendys, J. and Turley, M. [1983] - Results from the low-power, long-duration rotamak IV experiment. Paper presented at 14th AINSE Plasma Physics Conference, Lucas Heights, NSW.

Watt, G.C. [1983] - Rotamak vertical field driver type 645. AAEC Unpublished Technical Note AP/TN179.

TABLE 1
VARIOUS PLASMA PARAMETERS CALCULATED FOR ELECTRON TEMPERATURES OF 1 eV and 10 eV ASSUMING AN ELECTRON NUMBER DENSITY OF 3×10^{17} m^{-3} AND A NEUTRAL ATOM NUMBER DENSITY OF 1×10^{20} m^{-3}

Parameter	Unit	$T_e = 1$ eV	$T_e = 10$ eV
Debye length	m	1.4×10^{-5}	4.3×10^{-5}
No. of electrons in Debye sphere		3100	99 000
ν_{ei}	s^{-1}	8.9×10^{6}	3.8×10^{5}
ν_{en}	s^{-1}	2.8×10^{6}	8.9×10^{6}
δ, based on ν_{ei}	mm	12	2.5
δ, based on ν_{en}	mm	6.7	12
$\tau_{equilibration}$, argon	ms	4.0	96
$\tau_{equilibration}$ hydrogen	ms	0.1	2.4

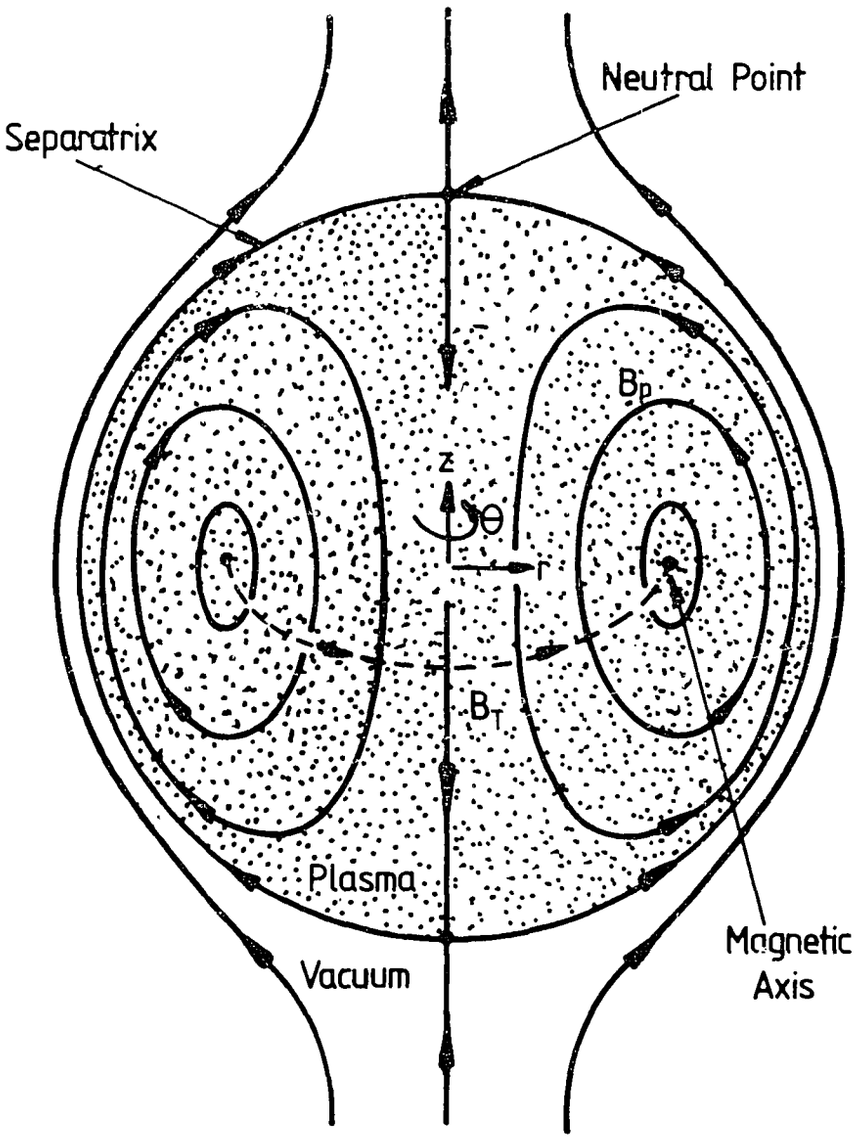

Figure 1 Magnetic field configuration of the rotamak. B_p is the poloidal magnetic field; B_T is the possible toroidal magnetic field. The rotating field has been omitted. The origin of the cylindrical coordinate system (r,θ,z) used in this report is also indicated.

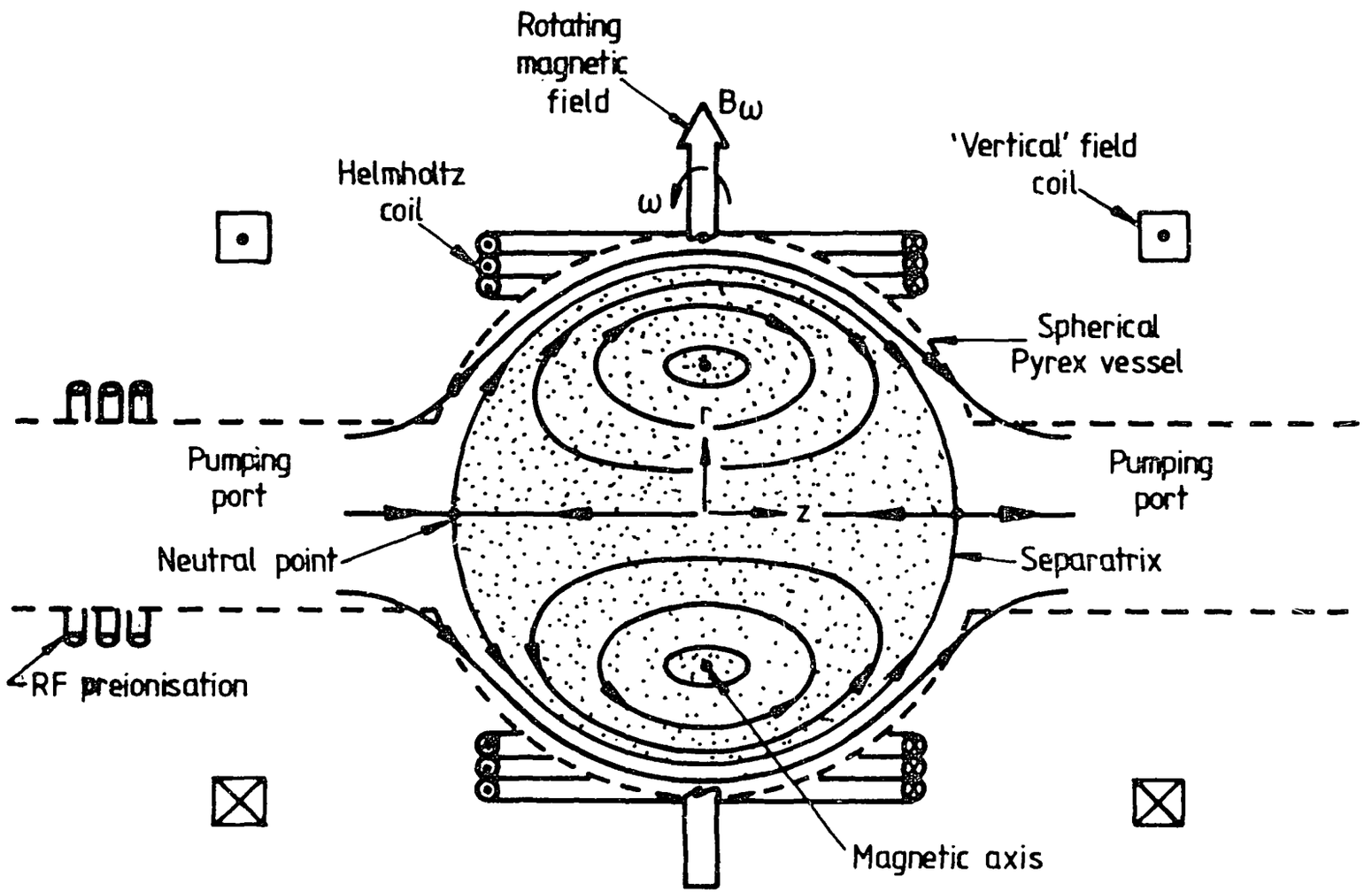

Figure 2a Schematic diagram of the experimental apparatus

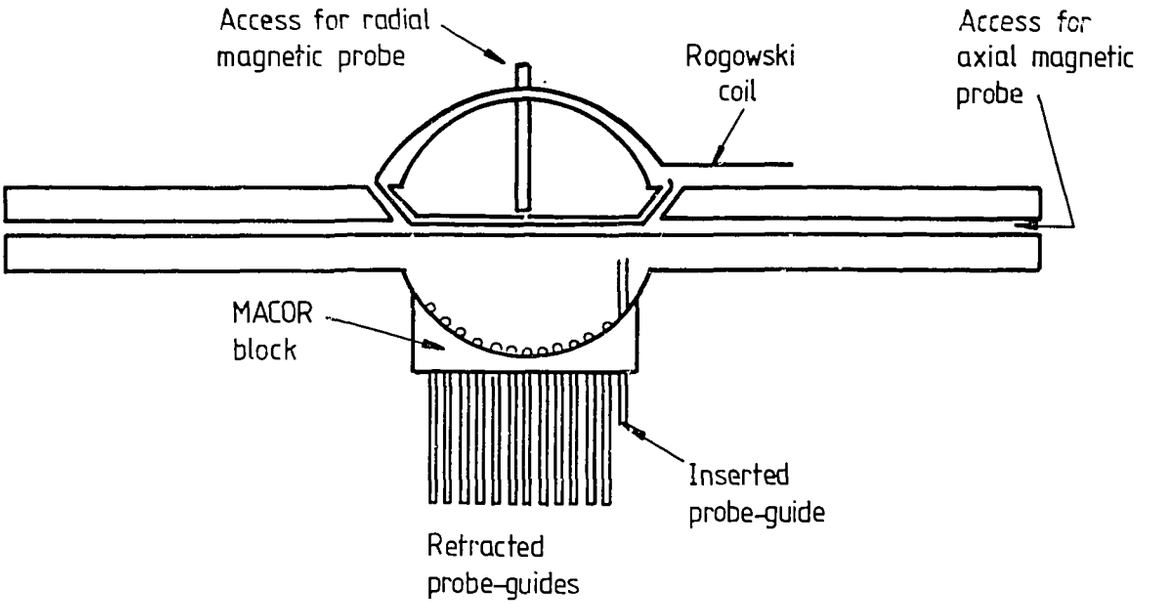

Figure 2b Location of Rogowski coil and magnetic probe guides

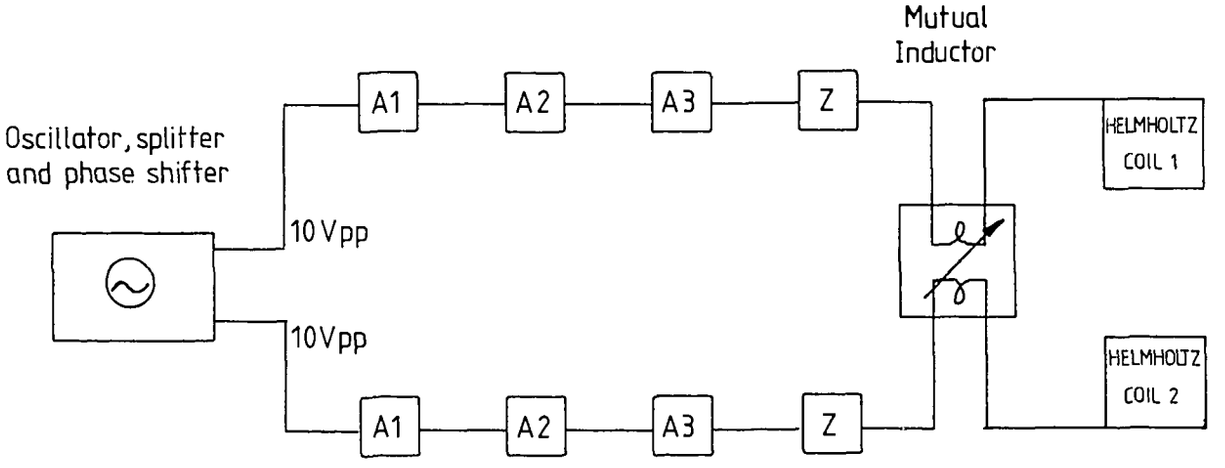

RF Amplifiers

A_1 : Spoken Type 250, Power Gain = 100

A_2 : YAESU FL 2100 Z, Power Gain = 6

A_3 : ETO ALPHA 77 Sx, Power Gain = 25

Z : Impedance Matching Circuit

Figure 3 Block diagram of the RF power amplifier system

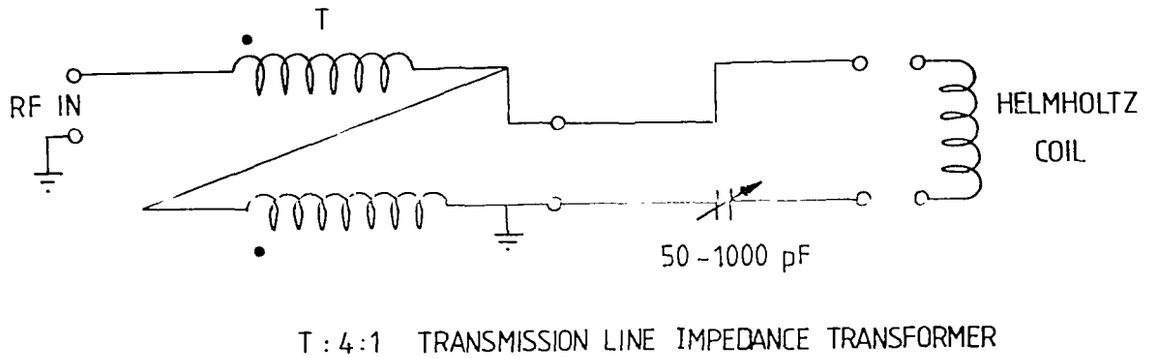

Figure 4 Diagram of the impedance matching circuit used to couple the RF amplifier to the Helmholtz coils.

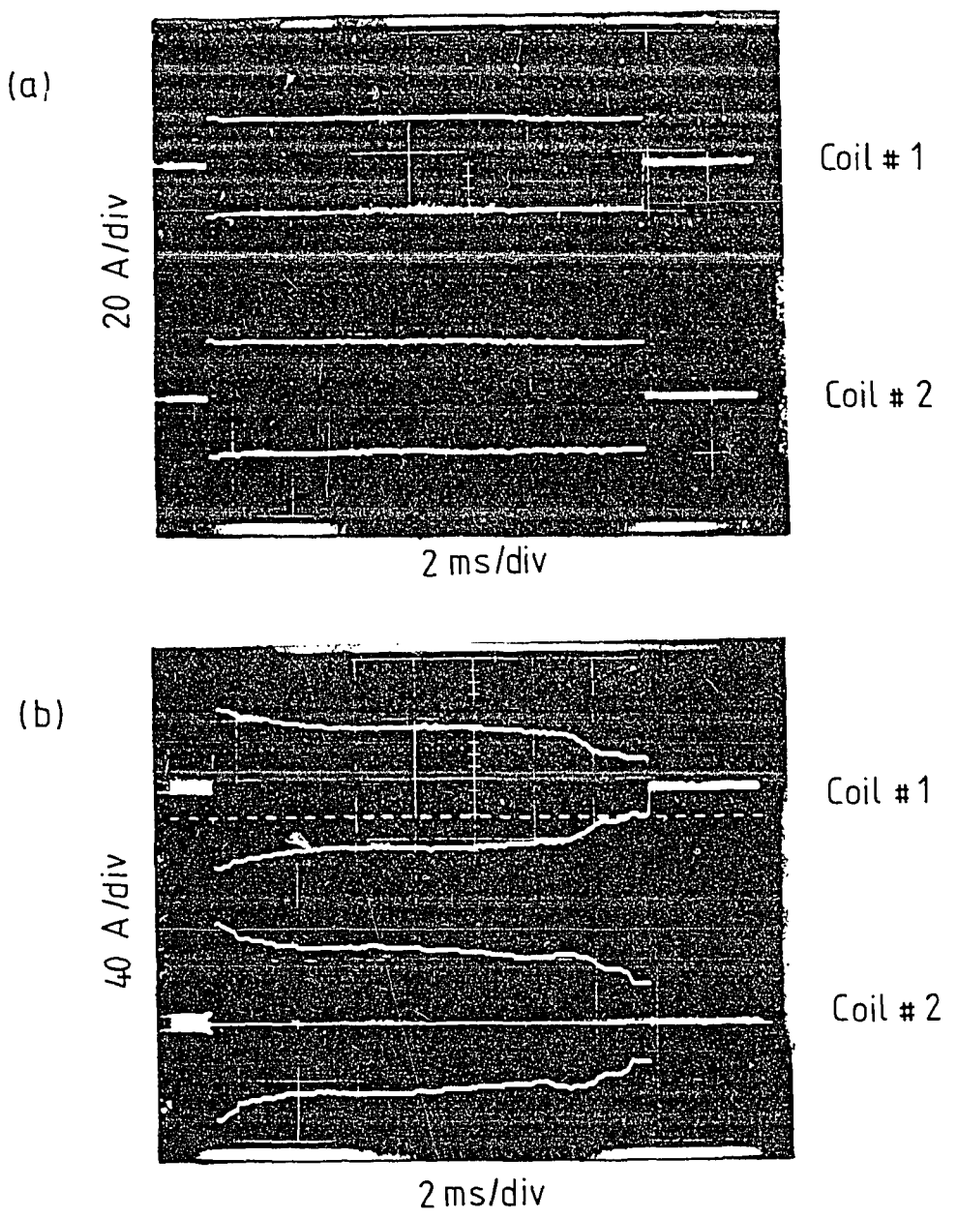

Figure 5 Typical envelopes of the RF current waveforms in the two Helmholtz coils: (a) vacuum discharge, and (b) hydrogen plasma discharge.

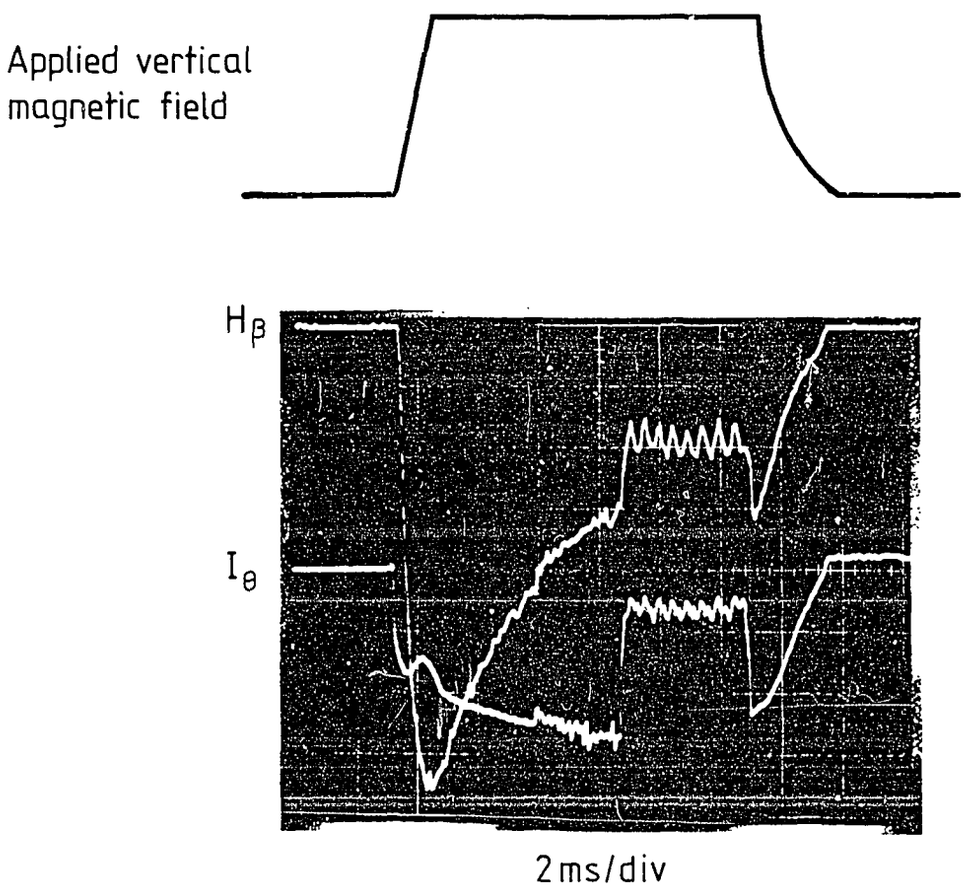

Figure 7 A discharge in which the driven current is partially cut off and then recovers. The lower trace shows the current I_θ (84 A/div). Note the fluctuations on the current trace which commence approximately 2 ms before cut-off. The upper trace is the intensity of the 486.1 nm spectral line. The initial hydrogen filling pressure is 190 mPa.

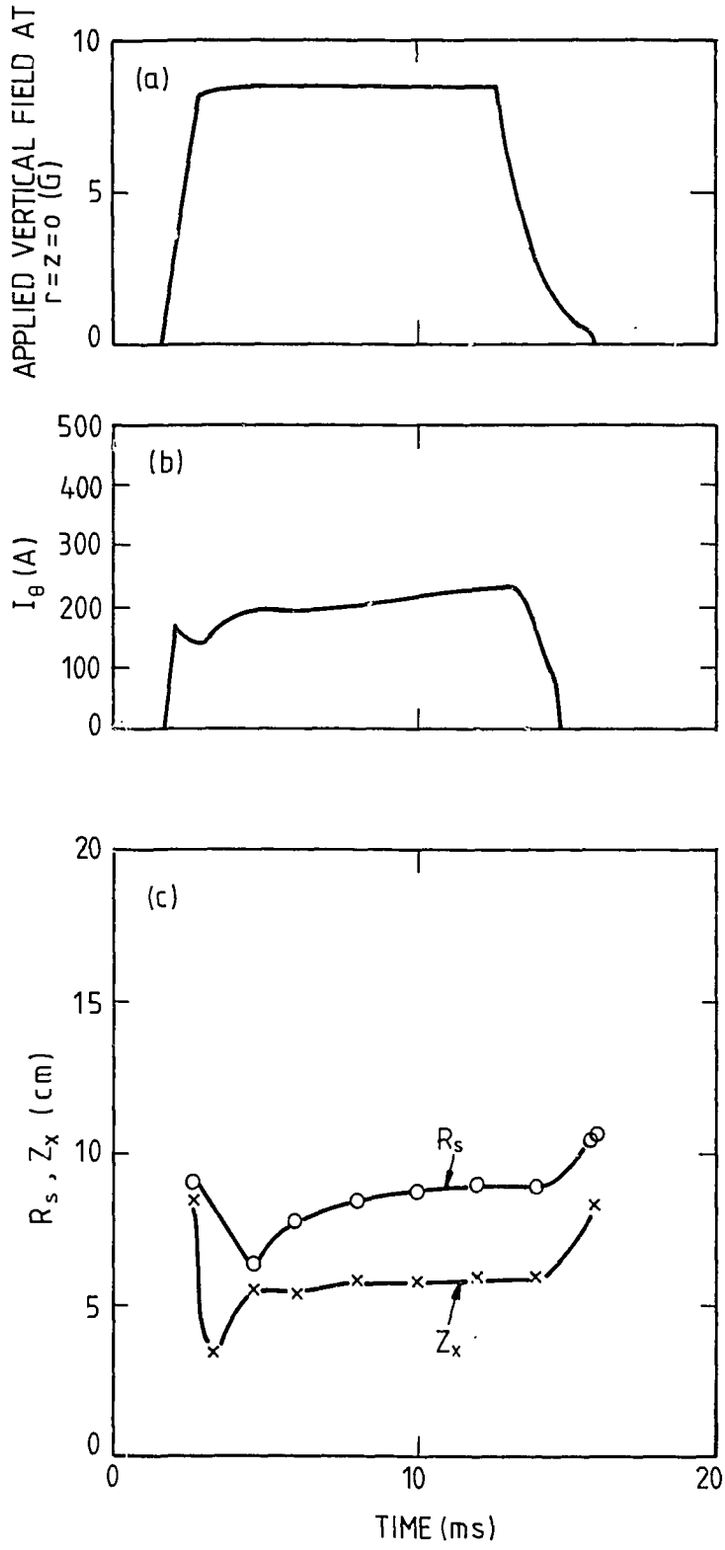

Figure 8 A typical hydrogen discharge (initial filling pressure, 160 mPa) showing (a) externally applied magnetic vertical field, (b) driven toroidal current, and (c) radial position of the separatrix, R_s and axial position of the neutral point, Z_x

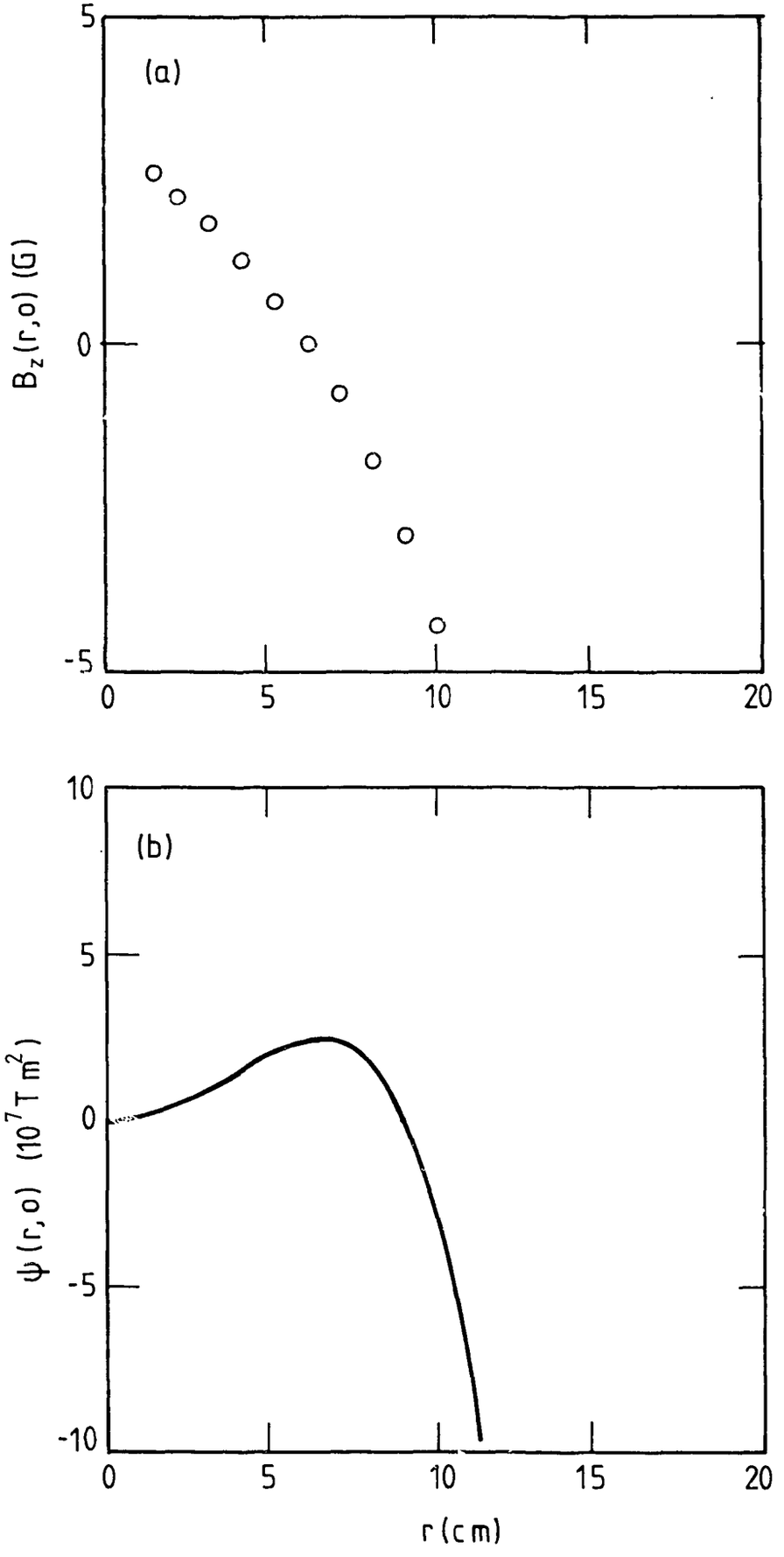

Figure 9 The radial distribution of $B_z(r,o)$ and the corresponding poloidal flux function, ψ, at 8 ms after the start of the discharge shown in figure 8

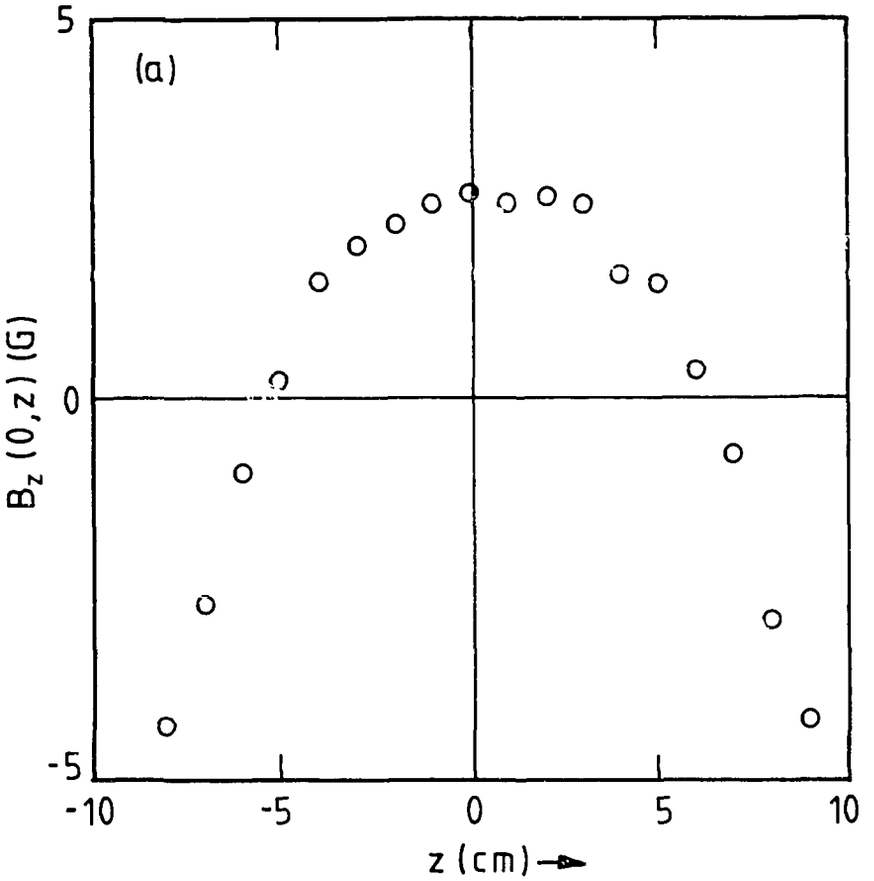

Figure 10 Axial distribution of B_z at 8 ms after the start of the discharge shown in figure 8

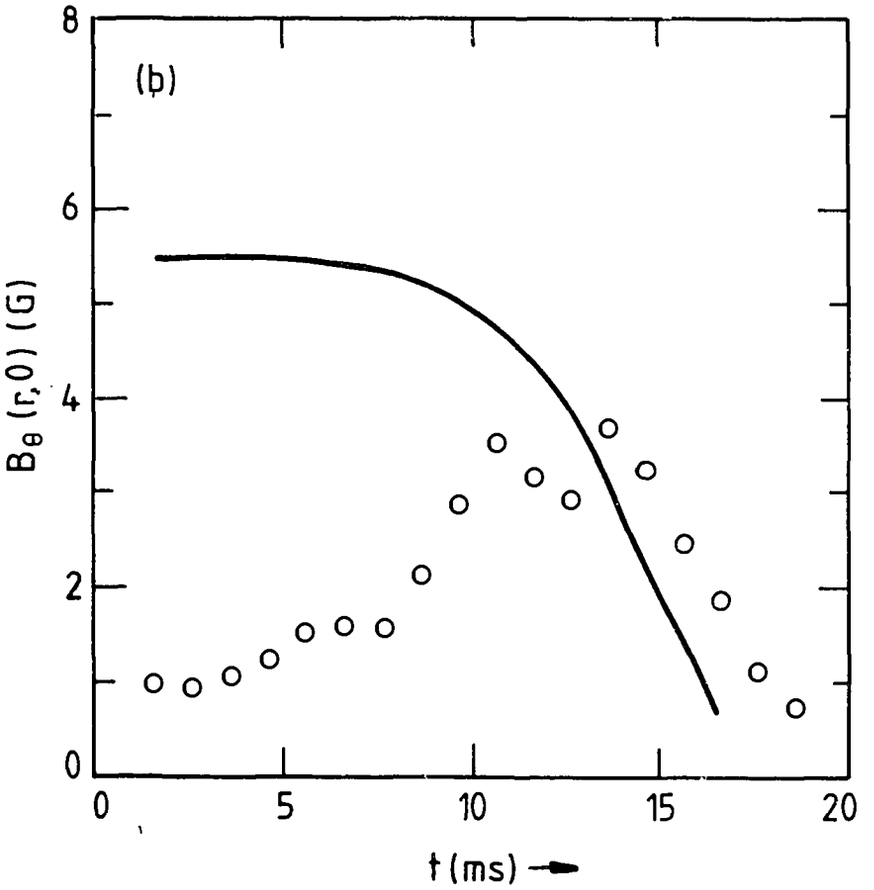

Figure 11 Radial distribution of B_θ at 8 ms after the start of the discharge shown in figure 8 (open circle). The solid line is the distribution in the absence of plasma

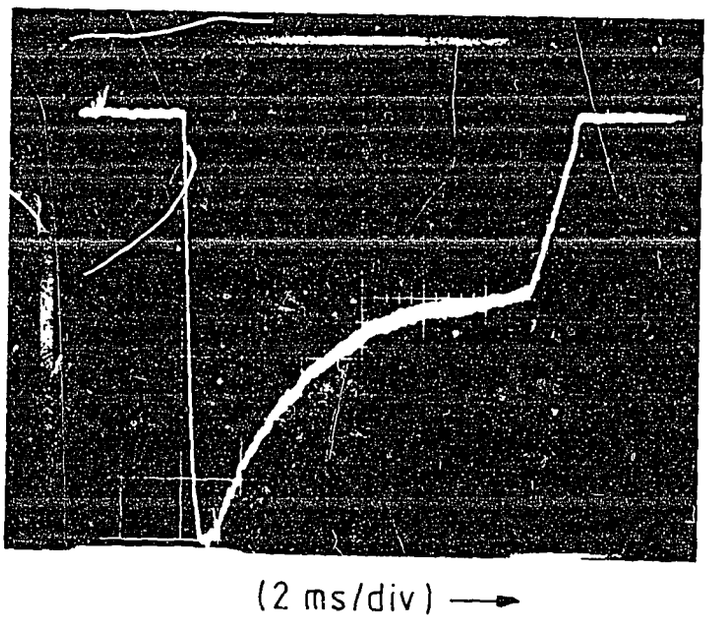

Figure 12 Relative intensity of 486.1 nm spectral line (H_β) as a function of time throughout the hydrogen discharge shown in figure 8

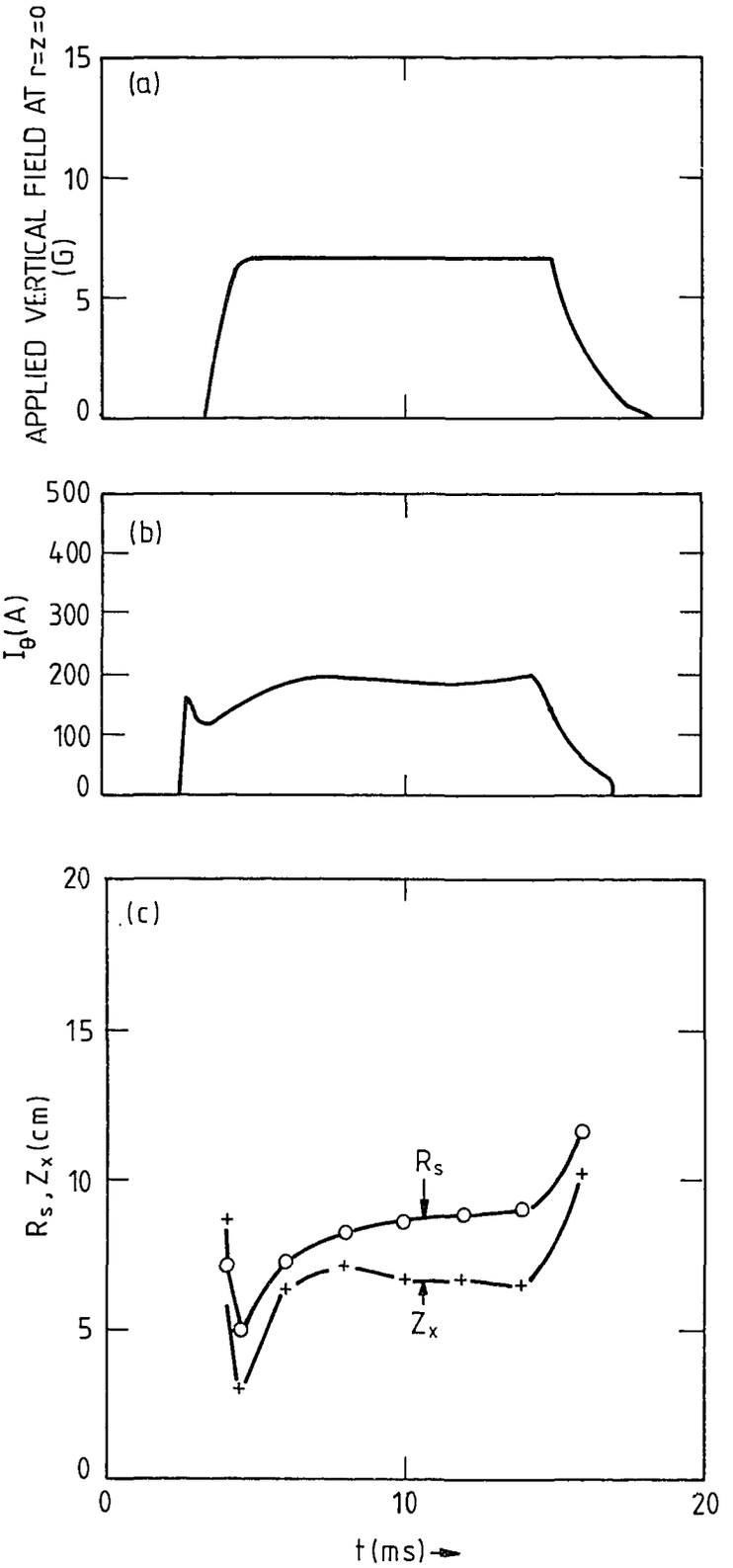

Figure 13 A typical deuterium discharge (initial deuterium filling pressure, 180 mPa) showing (a) externally applied vertical magnetic field, (b) driven toroidal current, and (c) radial position of the separatrix, R_s and axial position of the neutral point, Z_x

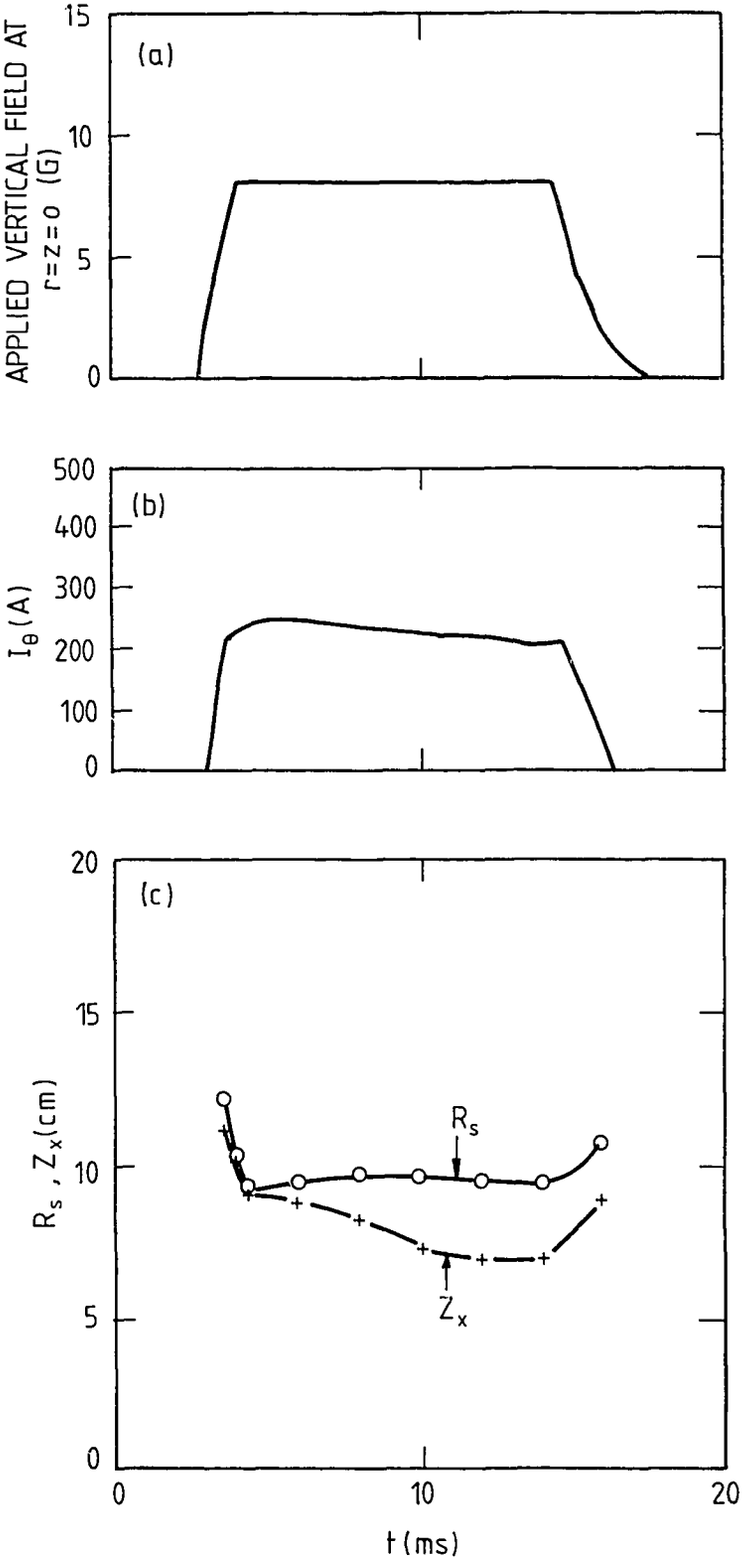

Figure 14 A typical helium discharge (initial helium filling pressure, 410 mPa) showing (a) externally applied vertical magnetic field, (b) driven toroidal current, and (c) radial position of the separatrix, R_s and axial position of the neutral point, Z_x

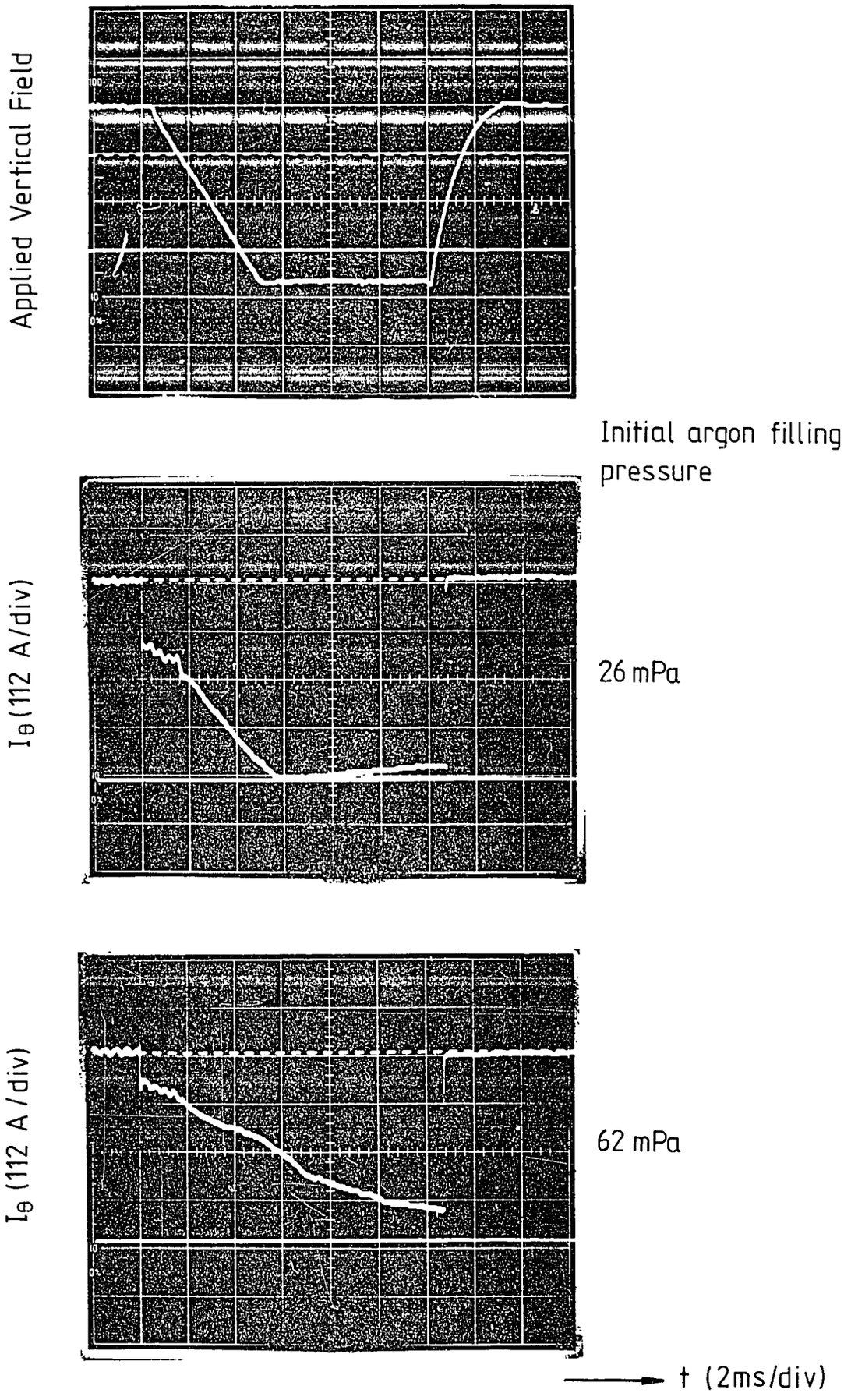

Figure 15 Effect of the initial filling pressure on argon discharges

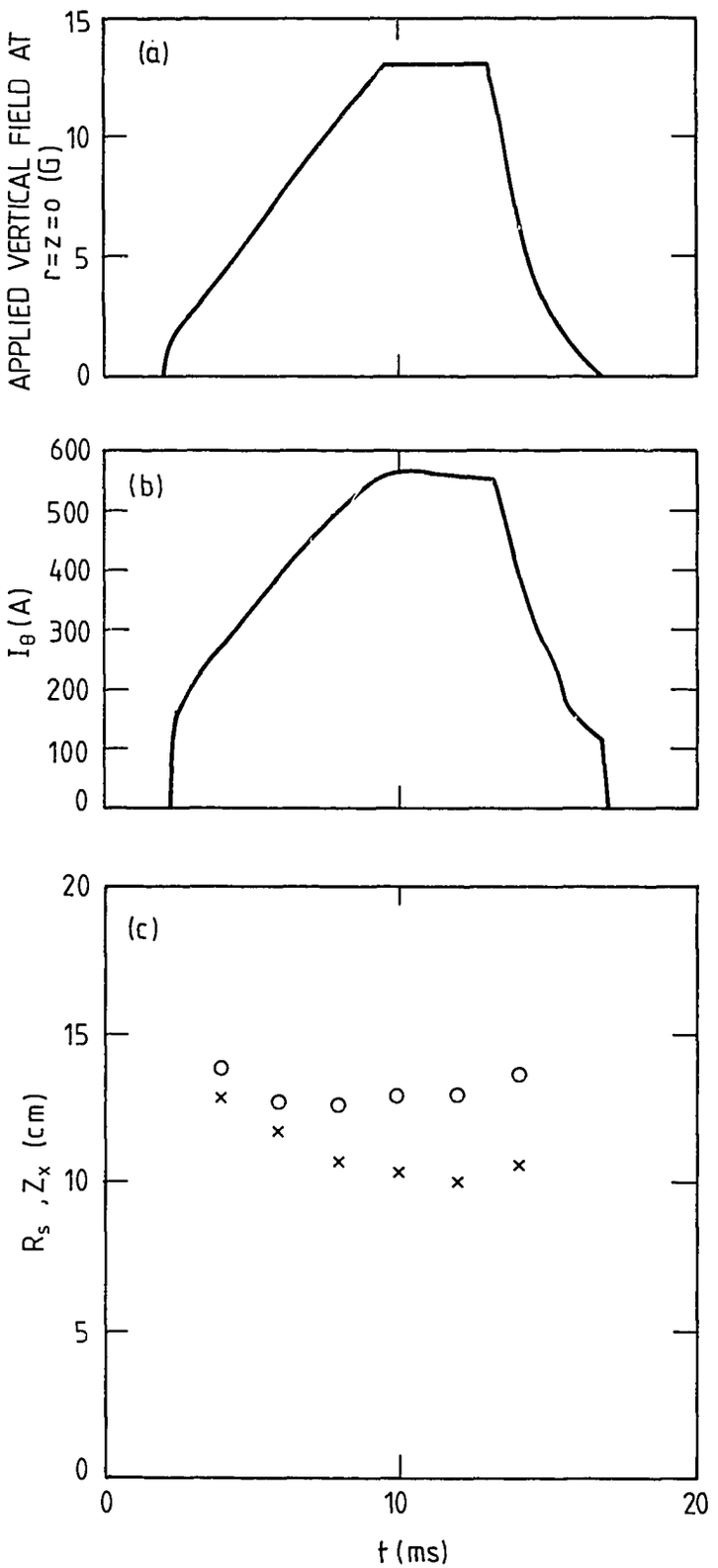

Figure 16 Typical argon discharge (initial argon filling pressure, 36 mPa) showing (a) externally applied vertical magnetic field, (b) driven toroidal current, (c) radial position of the separatrix, R_s and axial position of the neutral point, Z_x

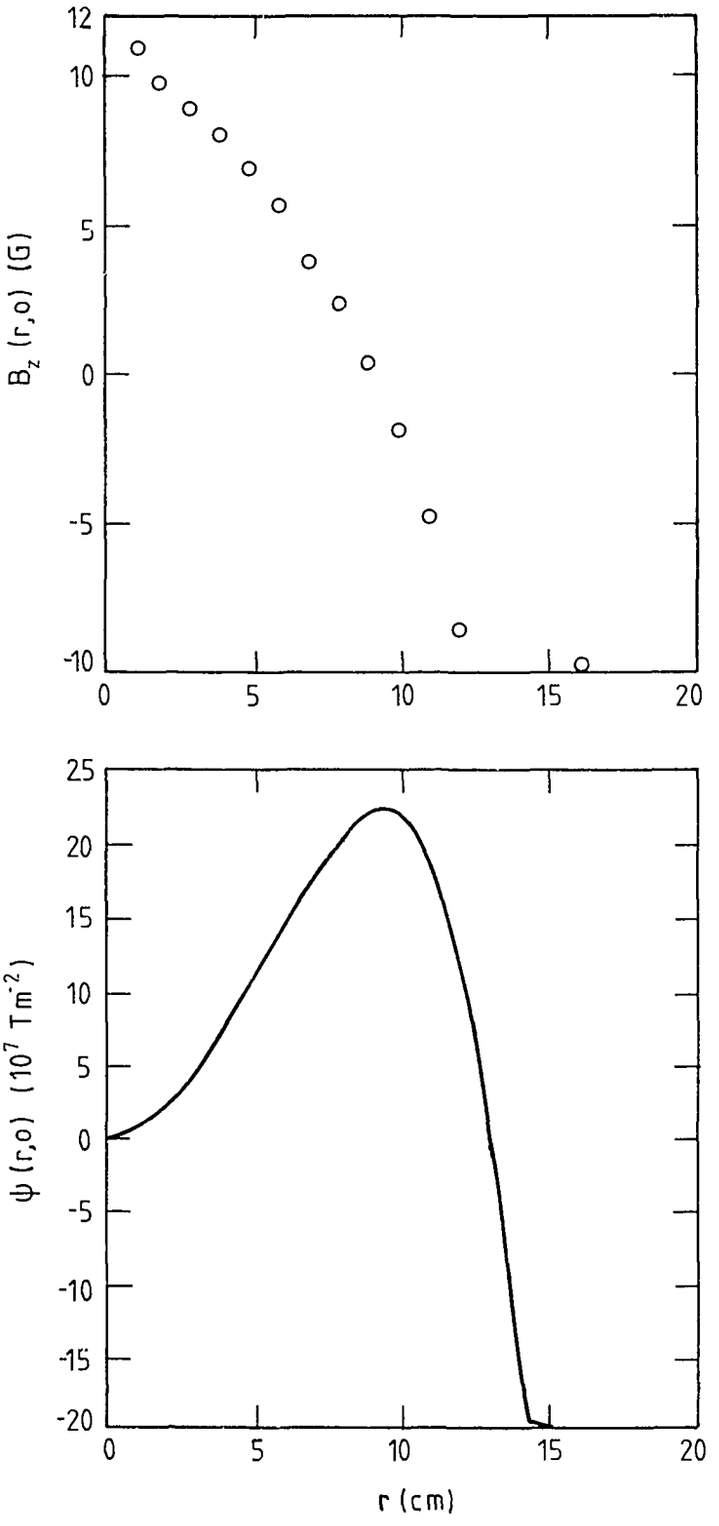

Figure 17 The radial distribution of B_z and the corresponding poloidal flux function, ψ, at 10 ms after the start of the discharge shown in figure 16

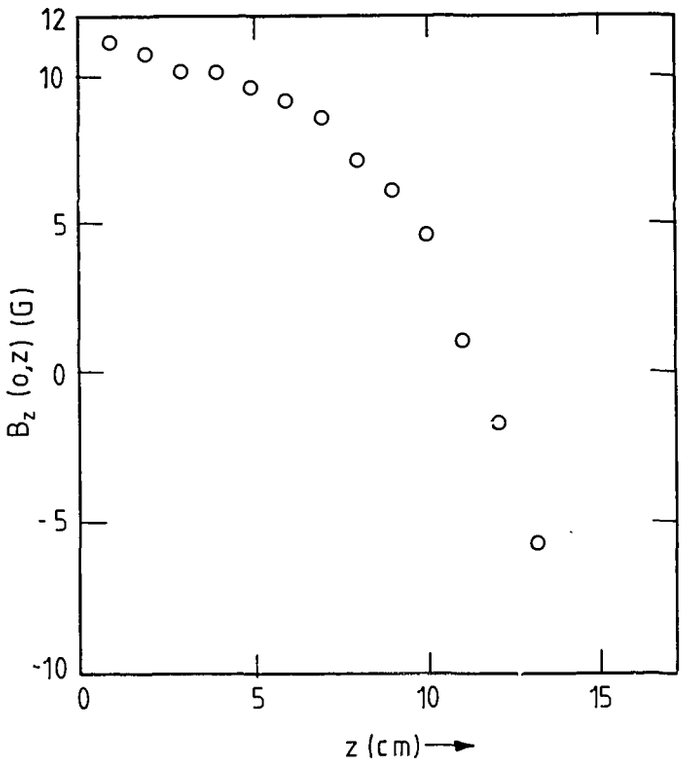

Figure 18 Axial distribution of B_z at 10 ms after the start of the discharge shown in figure 16

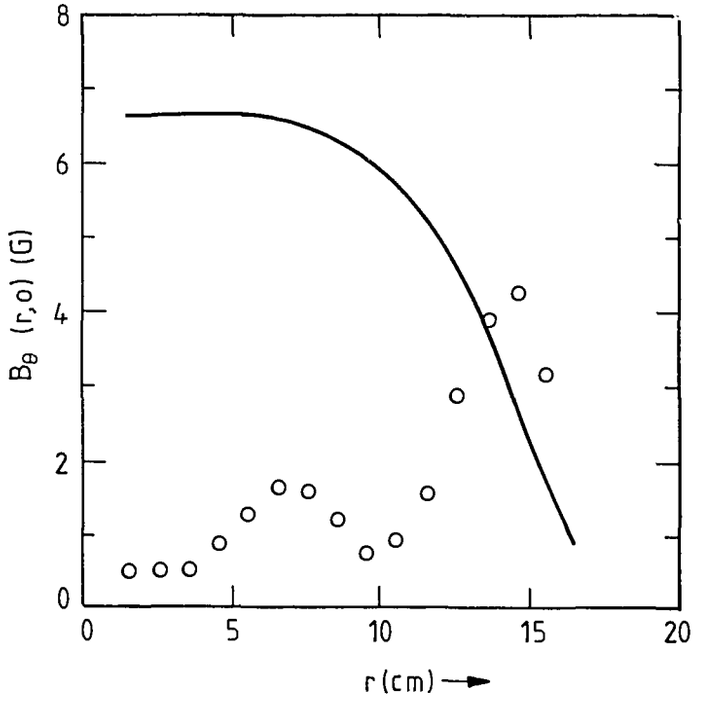

Figure 19 Radial distribution of B_θ at 10 ms after the start of the discharge shown in figure 16 (open circle). The distribution of plasma is shown by the solid line

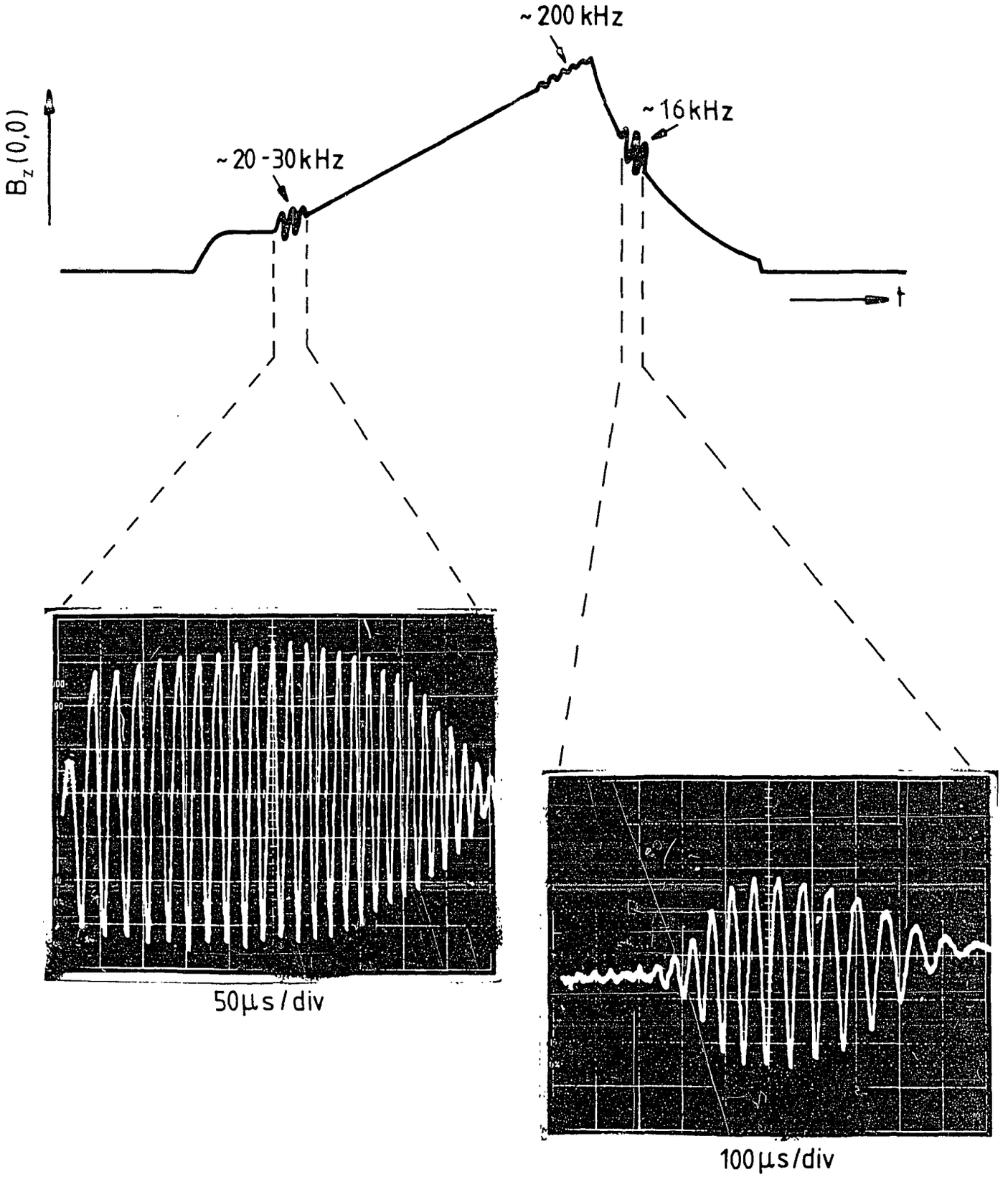

Figure 20 An illustration of the three regimes of oscillations observed in argon discharges. At the top is a diagrammatic sketch of the magnetic field at the centre of the plasma, while below are two photographs on an expanded time-scale of the fluctuations.

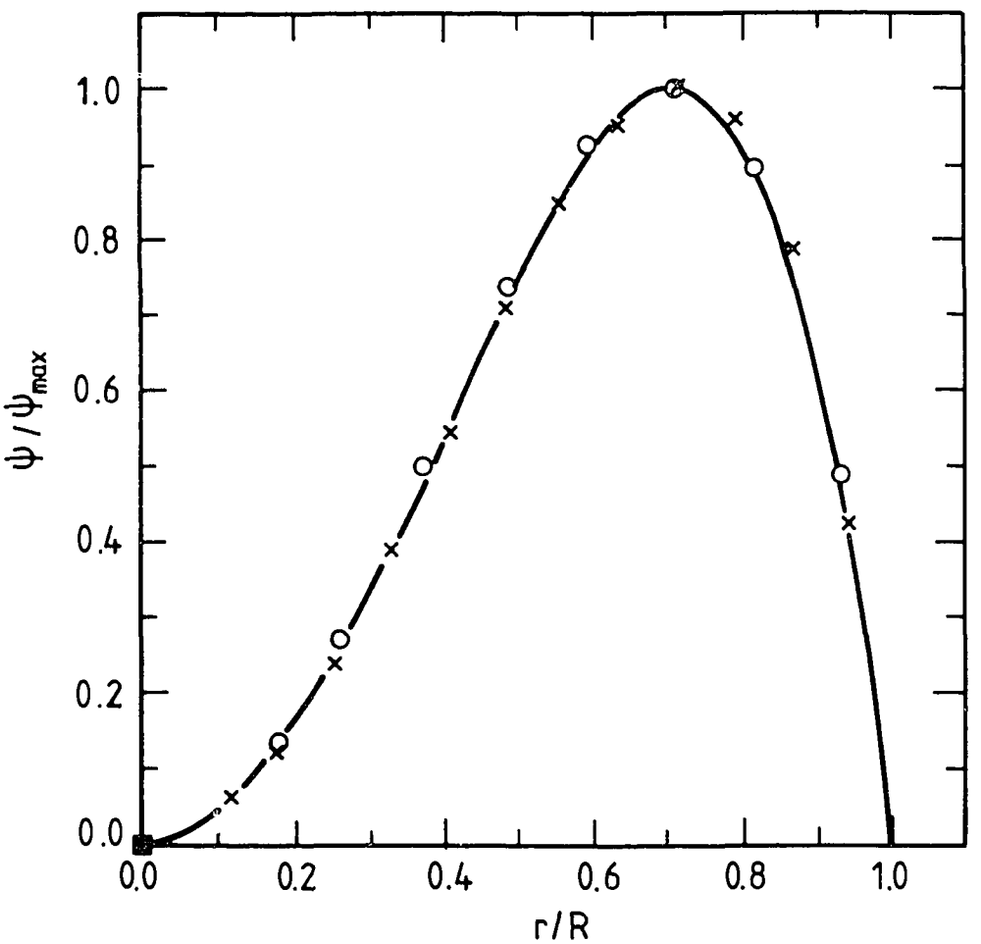

Figure 21 The function ψ/ψ_m versus r/R.
(—— Solov'ev model; o hydrogen; x argon)